

# Lawrence Berkeley National Laboratory

## LBL Publications

### Title

Simultaneous Enhancement in Electrical Conductivity and Thermopower of n-Type NiETT/PVDF Composite Films by Annealing

### Permalink

<https://escholarship.org/uc/item/2b15f0vs>

### Journal

Advanced Functional Materials, 28(37)

### ISSN

1616-301X

### Authors

Wolfe, Rylan MW  
Menon, Akanksha K  
Fletcher, Thomas R  
et al.

### Publication Date

2018-09-01

### DOI

10.1002/adfm.201803275

Peer reviewed

# Simultaneous Enhancement in Electrical Conductivity and Thermopower of n-Type NiETT/PVDF Composite Films by Annealing

Rylan M. W. Wolfe, Akanksha K. Menon, Thomas R. Fletcher, Seth R. Marder, John R. Reynolds, and Shannon K. Yee\*

Nickel ethenetetrathiolate (NiETT) polymers are promising n-type thermoelectric (TE) materials, but their insolubility requires the use of an inert polymer matrix to form films, which is detrimental to the TE performance. In this work, the use of thermal annealing as a post-treatment process simultaneously enhances the electrical conductivity from  $6 \pm 2$  to  $23 \pm 3$  S cm<sup>-1</sup> and thermopower from  $-28 \pm 3$  to  $-74 \pm 4$   $\mu$ V K<sup>-1</sup> for NiETT/PVDF composite films. Spectroscopic characterization reveals that the underlying mechanism involves removal of residual solvent and volatile impurities (carbonyl sulfide and water) in the NiETT polymer backbone. Additionally, microscopic characterization reveals morphological changes caused by a densification of the film that improves chain packing. These effects result in a 25  $\times$  improvement in power factor from 0.5 to 12.5  $\mu$ W m<sup>-1</sup> K<sup>-2</sup> for NiETT/PVDF films and provide insight into the composition of these coordination polymers that maintain their stability under ambient conditions.

techniques. There has been considerable effort recently in the area of organic TEs; however, much of this has focused on derivatives of poly(3,4-ethylenedioxythiophene)<sup>[1–4]</sup> that have high electrical conductivities,  $\sigma$ , but often suffer from a low Seebeck coefficient or thermopower,  $S$ . In contrast, organic n-type materials tend to have high  $S$  and low  $\sigma$  values,<sup>[5–7]</sup> necessitating the use of doping, which often drastically reduces the thermopower and can render the materials air sensitive. These results illustrate the inherent inverse correlation between these TE properties, and these trade-offs have been well studied in inorganic TE materials<sup>[8]</sup> within the framework of band-like transport.<sup>[9]</sup> Polymers, however, are unique in that the material performance is strongly determined by the processing conditions that

impact film morphology,<sup>[10,11]</sup> and transport is better described by thermally activated hopping conduction.<sup>[3,12,13]</sup>

Metal-coordination compounds, specifically metal-dithiolene coordination polymers, consisting of bridging ethenetetrathiolate ligands and nickel metal centers (nickel ethenetetrathiolate, NiETT), are one of the best-performing n-type organic TE materials. Pressed pellets of poly[K(NiETT)] have demonstrated high TE properties with  $S = -120$   $\mu$ V K<sup>-1</sup> and  $\sigma = 44$  S cm<sup>-1</sup> at room temperature, but the insoluble nature of the material limits its applicability.<sup>[14]</sup> One route to make NiETTs solution processable is by blending it with an inert matrix (e.g., poly(vinylidene fluoride), PVDF) and casting from low vapor pressure solvents (e.g., dimethyl sulfoxide, DMSO) albeit at the sacrifice of electrical conductivity.<sup>[15]</sup> Other strategies include fabricating composites with carbon nanotubes that yield high power factors, but the resulting material is often p-type.<sup>[16,17]</sup> This indicates the need for studying NiETTs further, and developing an n-type material that is both highly performing and solution processable. We have recently reported an optimized synthesis of Na[NiETT] that provides a reproducible material as validated by elemental analysis, X-ray photoelectron spectroscopy, and consistent TE properties across batches.<sup>[18]</sup> In that study, it was observed that thermal annealing composite films of ETT with PVDF/DMSO at ambient pressure resulted in a simultaneous increase in  $\sigma$  and  $S$ , thereby yielding power factors over 20  $\mu$ W m<sup>-1</sup> K<sup>-2</sup>; this represents a significant improvement (50  $\times$ ) over previous


## 1. Introduction

Thermoelectric (TE) devices use p- and n-type semiconducting materials for the conversion of heat into electricity. Compared with traditional inorganic semiconductors, organic materials based on conjugated polymers are promising for large-scale and low-cost thermal energy conversion because they can be processed from solution using inexpensive manufacturing

R. M. W. Wolfe, Prof. S. R. Marder, Prof. J. R. Reynolds  
School of Chemistry and Biochemistry  
School of Materials Science and Engineering  
Center for Organic Photonics and Electronics  
Georgia Tech Polymer Network  
Georgia Institute of Technology  
Atlanta, GA 30332, USA

Dr. A. K. Menon, Prof. S. K. Yee  
George W. Woodruff School of Mechanical Engineering  
Georgia Institute of Technology  
Atlanta, GA 30332, USA  
E-mail: shannon.yee@me.gatech.edu

Dr. T. R. Fletcher  
Cambridge Display Technology Ltd  
Unit 12, Cardinal Park, Cardinal Way, Godmanchester PE29 2XG, UK

 The ORCID identification number(s) for the author(s) of this article can be found under <https://doi.org/10.1002/adfm.201803275>.

DOI: 10.1002/adfm.201803275

reports which had a power factor of  $0.4 \mu\text{W m}^{-1} \text{K}^{-2}$  for these same blends.<sup>[19]</sup> Herein, we elucidate on mechanisms that occur during annealing these films that results in the simultaneous improvement of  $\sigma$  and  $S$ . Specifically, important morphological and chemical compositional changes are induced by annealing at  $160^\circ\text{C}$ . This observation also provides insight into the behavior and composition of these metal-coordination polymers. The effects of annealing NiETT have not been reported before, and these results suggest a novel pathway to increase the TE power factor of metal-coordination polymers.

## 2. Annealing Enhances Thermoelectric Properties

We refer the reader to our previous work on ETT optimization to obtain details on the synthesis parameters and reaction conditions (or see Experimental Section).<sup>[18]</sup> At the end of the synthesis, the reaction solution is vacuum filtered and the insoluble product dried under vacuum at room temperature for 24 hours to obtain NiETT particles in the form of a blue-gray lustrous powder (elemental analyses are given in Table S1, Supporting Information). Due to the insoluble nature of NiETT, films are fabricated by dispersing the particles in a  $10 \text{ mg mL}^{-1}$  solution of PVDF dissolved in DMSO. This mixture was then drop-cast on glass substrates and dried under vacuum for 30 min at  $50^\circ\text{C}$  to remove solvent resulting in films that are  $5\text{--}10 \mu\text{m}$  thick. This binder and solvent system is best suited for the formation of continuous composite films by drop-casting.<sup>[20]</sup> The films were subjected to a thermal annealing post-treatment process in air on a hot plate. To establish ideal annealing conditions, the temperature was varied for NiETT/PVDF films from  $80$  to  $160^\circ\text{C}$ . The processing and annealing conditions for the NiETT/PVDF composite films are expected to give  $\alpha$ -PVDF, which does not exhibit ferroelectricity.

The electrical conductivity and thermopower of composite films increase simultaneously with increasing annealing temperature up to  $160^\circ\text{C}$  (Figure 1). Annealing at higher

temperatures resulted in severe cracking of films and delamination from the substrate in many cases. The binder and film-forming polymer, PVDF, has a  $T_m$  of  $169^\circ\text{C}$ . Near and above this temperature, phase separation between NiETT and PVDF is observed. The conductivity increases from  $6 \pm 2 \text{ S cm}^{-1}$  for an as-cast film (control) to  $23 \pm 3 \text{ S cm}^{-1}$  upon annealing at  $160^\circ\text{C}$ ; this is accompanied by an increase in the Seebeck coefficient as shown in Figure 2 from  $-28 \pm 3$  (sample #1) to  $-74 \pm 4 \mu\text{V K}^{-1}$  (sample #2), to yield a power factor over  $10 \mu\text{W m}^{-1} \text{K}^{-2}$  for this n-type composite film. To test for air stability during annealing, additional films were annealed at  $160^\circ\text{C}$  in a vacuum and under nitrogen for 1 h – the resulting TE properties and elemental analysis were equivalent to air annealed samples, suggesting that there is no appreciable degradation (which would manifest as a significant reduction in TE properties and a change in elemental composition) or redox activity (which would manifest as a trade-off between conductivity and thermopower and a change in elemental composition) during the annealing process. The improvement in the electrical conductivity with annealing can be attributed to morphological changes, but the simultaneous enhancement in Seebeck is surprising. Thermogravimetric analyses (TGAs) show that annealing results in a 5% mass loss in NiETT powder and a 7% mass loss in the NiETT/PVDF film, indicating that different species may be evolved during the annealing process resulting in the enhancement in measured TE properties.

To isolate changes in NiETT powders from morphological changes in NiETT/PVDF composite films upon annealing, the NiETT powder was first annealed at  $160^\circ\text{C}$  for 1 h in air and then cast as a NiETT/PVDF thin film from DMSO yielding a material with a thermopower of  $-45 \mu\text{V K}^{-1}$  (Figure 2, sample #3). This is an improvement compared with the control film at  $-28 \mu\text{V K}^{-1}$  (Figure 2, sample #1) suggesting that a chemical change may be occurring in the NiETT powder when annealed. Upon annealing films prepared with these annealed powders (APs) at  $160^\circ\text{C}$  for 1 h in air, the magnitude of the thermopower further increases to  $-80 \mu\text{V K}^{-1}$  (Figure 2,

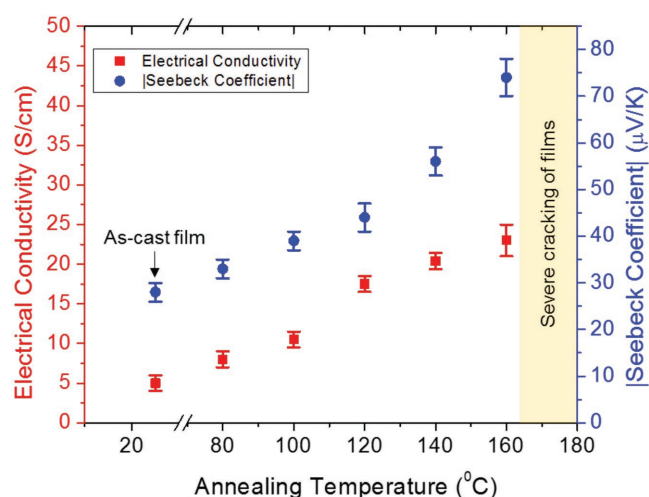


**Figure 1.** Electrical conductivity and Seebeck coefficient (magnitude) of NiETT/PVDF composite films as a function of annealing temperature. All films are annealed in air for 1 h on a hot plate prior to making TE measurements.

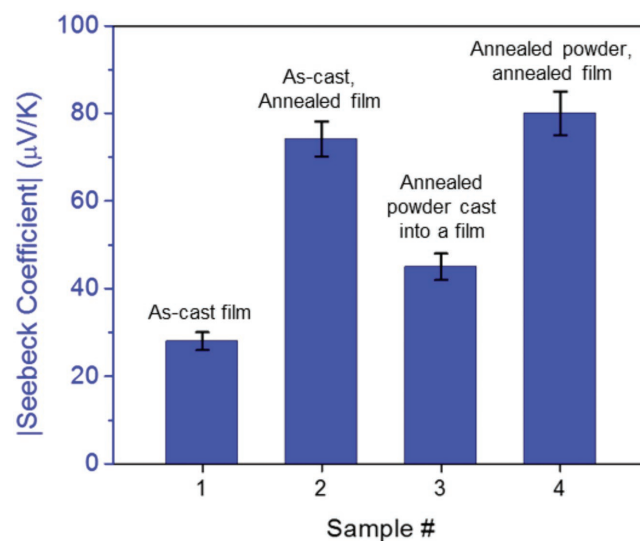


**Figure 2.** Seebeck coefficient (magnitude) of NiETT/PVDF composite films can be tuned by annealing the PP as well as the film. All samples are annealed in air for 1 h on a hot plate at  $160^\circ\text{C}$ .

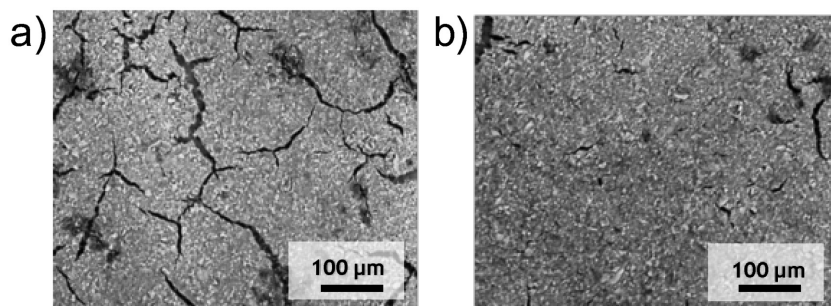


**Figure 3.** SEM images of NiETT/PVDF composite films a) before annealing and b) after annealing for 1 h in air at 160 °C.

sample #4). This reveals that the underlying mechanism for this enhancement is present in both the NiETT powder itself and in composite form with NiETT/PVDF films.

### 2.1. Annealing Changes Film Morphology

It is known that favorable interaction between the binder and solvent could significantly impact the amount of residual solvent in the film. Given that DMSO is a hygroscopic, low vapor pressure solvent, vacuum drying for 30 min may not remove all the solvent. **Figure 3** shows SEM images of a NiETT/PVDF film before and after annealing. During the annealing post-treatment process, some of this residual solvent is removed which causes a densification of the film and closes existing cracks (potentially formed from thermal stresses during the original vacuum drying process) present toward the center of the film; some cracks are still observed toward the edges of the film. Annealing just below the melting temperature of PVDF (i.e., at 160 °C, see Figure S1, Supporting Information) allows NiETT to reorganize into more well-connected domains. Similar observations have been made with carbon nanotubes in an inert matrix, where the filler reorganizes into more conducting pathways upon annealing.<sup>[21,22]</sup> This morphological effect is reflected in a higher  $\sigma$  for annealed NiETT/PVDF films compared with as-cast films. However, an increase in the thermopower is also observed, which cannot be explained by reorganized conducting pathways alone; this suggests that another mechanism is present during the annealing process. We hypothesize that annealing results in the removal of volatile impurities in addition to the observed morphological effects, and tandem TGA–mass spectrometry (TGA–MS) was employed to gain insight into species that are evolved during this annealing process.

### 2.2. Annealing Changes Material Composition

TGA indicates that four mass-loss events (Events A–D) occur in the NiETT powder and in the NiETT/PVDF composite films during heating to 600 °C (see Figure S2, Supporting Information, for TGA temperature profile; see Figures S3–S6, Supporting Information, for full ion signals). Event A, mimicking the annealing conditions, occurs upon heating to and holding

at the annealing temperature of 160 °C for 1 h. Event B begins at  $\approx 190$  °C and shows a peak mass-loss rate at  $\approx 235$  °C, indicating significant decomposition of the polymer at these temperatures. Event C (peak loss rate at 385 °C) and Event D (peak loss rate at 595 °C in powders, 470 °C in films) are attributed to continued decomposition of NiETT and PVDF. Mass-loss Event A is critical to understanding the effect of annealing on NiETT powders and NiETT/PVDF composites.

First, NiETT powder in its original state (pristine powder, PP) and NiETT powder after annealing at 160 °C for 1 h in air annealed powder (AP) are considered (**Figure 4**). In

these samples, the onset of mass loss is as early as 50 °C (the full duration at half-maximum, FDHM, of the derivative thermogravimetry (DTG) curve is used to identify the temperature range of each event). While this corresponds to the vacuum drying temperature of the films, water is the only signal active at 50 °C. In PP, Event A is a broad, shallow loss that begins at 70 °C and ends during the isothermal hold, and **Figure 4a** shows two species are evolved – water and carbonyl sulfide – contributing to a total mass loss of 5.3%. The presence of water is expected as mass losses up to 7% have been previously attributed to water in NiETTs.<sup>[23]</sup> However, this is the first reported observation of an impurity or decomposition product such as carbonyl sulfide being removed upon annealing a NiETT polymer. The water evolved is hypothesized to be contact moisture; the heating rate ( $10 \text{ K min}^{-1}$ ) prevents differentiation between water removed at or below the boiling point (surface or contact moisture) and water removed above the boiling point (incorporated water). For example,  $\text{NiSO}_4 \cdot 6\text{H}_2\text{O}$  shows incorporated water removed at 100–220 °C and  $>300$  °C<sup>[24]</sup>;  $\beta\text{-Ni(OH)}_2$  shows surface moisture removed at 80–90 °C, and incorporated water removed at 160 °C; and  $\alpha\text{-Ni(OH)}_2$  shows incorporated water removed at 240–300 °C.<sup>[25]</sup> The second component, carbonyl sulfide, is an unexpected decomposition product when considering the ideal atomic composition  $\text{Na}_x[\text{Ni}(\text{C}_2\text{S}_4)]_n$  for these polymers. The source of this signal is potentially from unreacted carbonyl end groups or sulfonyl irregularities<sup>[26]</sup> in the polymer backbone. Previous elemental analyses and X-ray photoelectron spectroscopy (XPS) data support the presence of such impurities.<sup>[18]</sup> Even in carefully controlled syntheses, impurities and deviations from the idealized structure are present and should be expected.

In AP, Event A consists of a 2.8% mass loss during annealing, as shown in **Figure 4b**, and the signal from carbonyl sulfide is significantly reduced compared with PP. Water, specifically contact moisture, is the major contributor to the 2.8% mass loss, along with small amounts of carbonyl sulfide as evidenced from the MS ion traces for AP. Therefore, the mass loss in PP (5.3%) is approximated to be  $\approx 2.8\%$  contact moisture and  $\approx 2.5\%$  carbonyl sulfide. This highlights the importance of proper reaction and work-up conditions as well as material post-treatment as removing a small amount of impurity (e.g., carbonyl sulfide) by annealing the NiETT powder increases the thermopower from  $-28$  to  $-42 \mu\text{V K}^{-1}$  when cast into a film.

Event B (203–288 °C FDHM), in both PP and AP, begins the irreversible and destructive decomposition of the NiETT

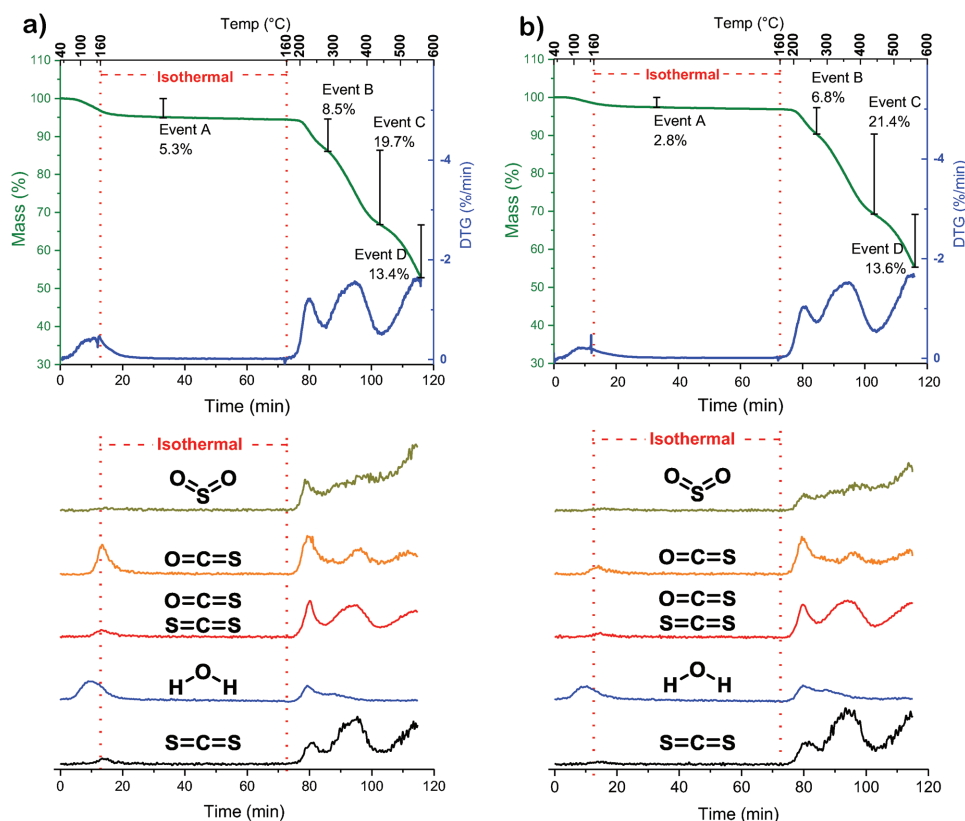


**Figure 4.** TGA with tandem MS of PP and AP samples of NiETT. a) TGA with plotted differential (DTG) of PP and normalized ion signals from QMID, b) TGA with plotted DTG of AP and normalized ion signals from QMID. See Figures S1 and S2 in the Supporting Information for additional data.

polymer. The onset temperature (180 °C) is recommended as the maximum temperature for any processing method (e.g., annealing, printing, extruding) for NiETT. Event B evolves additional water and carbonyl sulfide and begins the release of sulfur dioxide and carbon disulfide. As no combustion is taking place, the water released is expected to originate from incorporated water. The strong signal in Event B from carbonyl sulfide alongside the signals from sulfur dioxide and carbon disulfide indicates that carbonyl sulfide is released as both a beneficial removal of impurities (Event A) and as a destructive decomposition of the NiETT backbone (Event B). The presence of sulfur dioxide provides additional evidence of sulfonyl groups in the backbone, as it is evolved at a lower temperature (200 °C) than sulfur dioxide from NiSO<sub>4</sub> decomposition (>700 °C).<sup>[27]</sup> The start of evolution of carbon disulfide indicates that the main backbone of NiETT is decomposing at these elevated temperatures. Event C (288–444 °C) is a continuation of Event B, and releases additional carbon disulfide, hydrogen sulfide, and sulfur dioxide. The final decomposition, Event D (515–600 °C), continues to the end of the run releasing carbon disulfide, sulfur dioxide, hydrogen sulfide, and water. Based on these observations from TGA-MS, we hypothesize some additional structures that are likely present in these NiETT polymers, shown in **Figure 5**. Elemental analysis

confirms the chemical compositional changes observed in the TGA-MS experiment (see Table S1 Supporting Information).

Extending the analysis to composite films, **Figure 6** shows the TGA-MS curves with associated ion signals for two film samples: a NiETT/PVDF film cast from DMSO (pristine film, PF) and a NiETT/PVDF film cast from DMSO that is annealed at 160 °C in air for 1 h (annealed film, AF). As in the powder samples, the films show four mass-loss events, denoted as Events A–D. The signal-to-noise ratio is decreased in these samples due to the small mass of an individual film. We note that the NiETT powder used in both these films is not annealed (similar to PP discussed earlier). For both film samples, Event A (≈80–160 °C) aligns with the annealing process, and is crucial for obtaining high TE properties. Event B (206–266 °C) and Event C (346–438 °C) are the major NiETT decomposition events that occur after annealing. Both have similar FDHM and

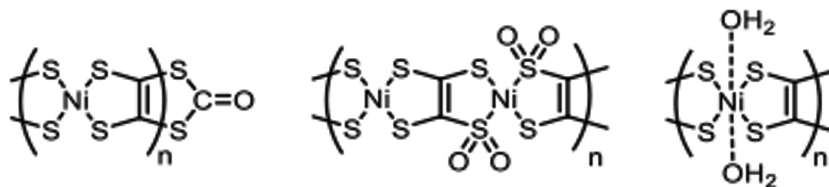


**Figure 5.** Possible structures present in NiETT that give rise to carbonyl sulfide, water, or sulfur dioxide signals. These are in contrast to the idealized backbone represented by Na<sub>x</sub>[Ni(C<sub>2</sub>S<sub>4</sub>)<sub>n</sub>] found in the literature.



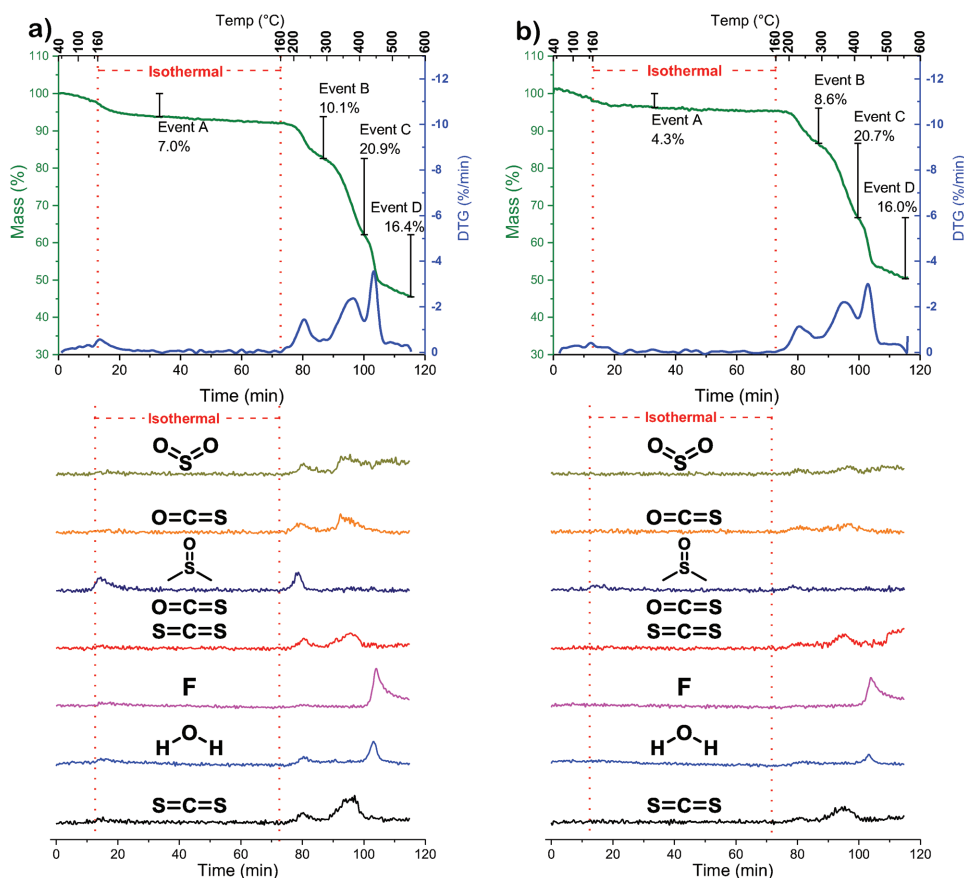


**Figure 6.** TGA with tandem MS of PF and AF samples of NiETT/PVDF/DMSO. a) TGA with plotted differential (DTG) of PF and normalized PF ion signals from QMID, b) TGA with DTG of AF and normalized AF ion signals from QMID. See Figures S3 and S4 in the Supporting Information for additional data.

peak mass-loss temperatures as the powders, confirming that this is a NiETT decomposition. Event D (440–487 °C) occurs at a lower temperature in the films that is consistent with the decomposition onset of PVDF (Figure S7, Supporting Information). In PF, the mass loss in Event A totals 7.0% and shows a weak signal of water and almost no signal of carbonyl sulfide when compared with the powder samples. The most prominent mass-loss signal during this step is from DMSO. Beyond Event A, during the isothermal hold, there is an additional 1.7% mass loss in PF that is believed to be the slow release of DMSO from the film. In contrast, in AF, Event A consists of a smaller mass loss of 4.3%, with no discernable water or carbonyl sulfide signals; the most prominent ion signal is also from DMSO. Less surface moisture is expected to return to the films compared with the powders upon exposure to atmosphere after annealing, as the hydrophobic PVDF surrounding the NiETT particles prevents reabsorption of water. Vacuum drying films at 50 °C for 30 min followed by annealing for 1 h at 160 °C does not fully remove DMSO from the composite films. However, complete removal of DMSO is not required to realize the full enhancement in TE performance.

As with the powder samples, Event B in both films (PF and AF) reveals the loss of sulfur dioxide and carbon disulfide from the decomposition of NiETT. The signal for water is minimal in PF and indiscernible in AF, and instead, a signal for DMSO

is observed in both. The DMSO released in Event B originates from a separate source more strongly bound within the film (analogous to the incorporated water in PP and AP), as compared with the DMSO released in Event A (which is DMSO trapped within the PVDF). We hypothesize that, in the NiETT powder form, water is bound to both the particle surface and to nickel centers, either in the backbone of the NiETT or as impurities in the film. Annealing the powder removes surface moisture (Event A signals) but does not remove the more strongly bound hydrates (Event B signals). In these powder samples, the surface moisture is rapidly replaced upon cooling in atmosphere causing a similar water signal in both PP and AP in Event A. During the film fabrication process, NiETT experiences a saturated DMSO environment, and contact moisture moves from the surface into the bulk solution. Water bound to nickel centers, both main chain and impurity hydrates, is also exchanged for DMSO. This results in the formation of a nickel–DMSO complex in the composite film.<sup>[28]</sup>

When both film samples (PF and AF) are dried at 50 °C under vacuum, the contact moisture and previously bound water are removed along with the majority of the DMSO. Some DMSOs remain trapped in the PVDF film and is released in PF – Event A, and additional DMSO is bound to nickel centers and is released in PF – Event B. For AF, DMSO trapped within the PVDF matrix is readily removed, as evidenced by the rapid

decline of DMSO ion signal in AF – Event A, and the DMSO signal in AF – Event B is significantly smaller than PF – Event B. This suggests that the process of removing DMSO from the film helps drive the film reorganization, which manifests as a boost in electrical conductivity. Event C in AF and PF shows the same evolution of carbon disulfide and sulfur dioxide as the powder samples, suggesting the NiETT polymer is unaffected by processing into a composite. Event D shows a spike in the fluorine signal that matches well with the decomposition of neat PVDF.

For the fabrication of TE devices using NiETT, alternative binders beyond PVDF may be required to address issues such as ink viscosity and solvent compatibility. A preliminary study suggests that the efficacy of annealing is highly dependent on the choice of binder–solvent system used to disperse NiETT particles – solubility, glass transition and melting point, crystallinity, and interaction with NiETT are different factors that may impact the annealing conditions and TE properties. As such, a systematic study of binder and solvent systems could provide further understanding of this mechanism.

### 3. Charge Transport in NiETT/PVDF Films

Temperature-dependent  $S$  and  $\sigma$  measurements were performed to elucidate the charge transport mechanism in annealed NiETT/PVDF composite films. Figure 7 shows the electrical conductivity and Seebeck coefficient magnitude for Na(NiETT) films as a function of temperature.

The electrical conductivity increases with temperature indicating that the transport is thermally activated. In this temperature range, the Seebeck coefficient increases slightly but this increase is within measurement uncertainty limits. Temperature-dependent properties of NiETT/PVDF films prior to annealing follow the same trend as that shown in Figure 7 albeit with lower  $S$  and  $\sigma$  values. This is indicative of semiconducting behavior and follows hopping conduction, as expected for disordered materials. Fitting the temperature-dependent data to Mott's variable range hopping model yields a linear fit for a 3D system (Figure S8, Supporting Information). However,

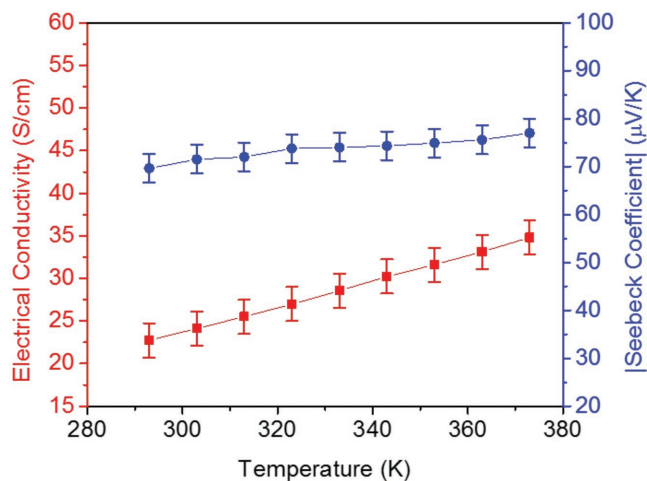


**Figure 7.** Temperature-dependent TE properties of annealed NiETT/PVDF films are indicative of thermally activated hopping transport.

percolation mechanisms also show a similar power-law conductivity dependence, which may be a more accurate description of charge transport in NiETT/PVDF composites due to sample inhomogeneity. Low-temperature  $S$  and  $\sigma$  measurements coupled with gated measurements may be required to fully elucidate the transport mechanism in these materials.

### 4. Conclusion

NiETT/PVDF is a promising air-stable n-type TE material. This work investigates the use of an annealing post-treatment process to enhance the performance of NiETT/PVDF thin films cast from DMSO. While we previously demonstrated the reproducibility between batches and batch sizes,<sup>[18]</sup> nonetheless a single batch of Na(NiETT) was selected for all annealing studies to remove any possible differences in particle size or composition. The TE properties were simultaneously enhanced upon annealing composite films, and are attributed to i) improved film morphology and ii) compositional changes in the NiETT material. TGA-MS reveals the reversible removal of water (as contact moisture and incorporated in the polymer backbone) and the irreversible removal of carbonyl sulfide upon annealing NiETT powder. For PP, removal of  $\approx 3\%$  mass, corresponding to carbonyl sulfide as an impurity, results in an increase in the thermopower from  $-28$  to  $-42 \mu\text{V K}^{-1}$ . For the films, TGA-MS indicates that DMSO is the major contributor to mass loss during the annealing process; the solvent replaces both contact moisture and incorporated water in NiETT during film fabrication. Annealing near the melting point of the binder (PVDF) could allow for reorganization of domains to form highly interconnected pathways that increases the conductivity from 6 to  $23 \text{ S cm}^{-1}$ . The removal of moisture, residual solvent, and impurities through annealing works in tandem with the thermal- or solvent-driven morphological changes to yield a  $25 \times$  increase in power factor from  $0.5 \mu\text{W m}^{-1} \text{ K}^{-2}$  in PFs to  $12.5 \mu\text{W m}^{-1} \text{ K}^{-2}$  in AFs that maintain their stability under ambient conditions.

### 5. Experimental Section

**Polymer Synthesis:** A single batch of Na[Ni(ETT)], prepared according to our recent literature procedure, was used for all experiments.<sup>[18]</sup> In a cool, dry roundbottom flask with magnetic stir bar, thiapendione (500 mg, 2.4 mmol, 1.0 equiv) was added against a positive flow of argon. The atmosphere was thoroughly purged with argon. Anhydrous, degassed MeOH (15 mL) was added by syringe, and the reaction was heated to  $60 \text{ }^\circ\text{C}$ . Separately, NaOMe (648 mg, 12 mmol, 5.0 equiv) was dissolved in MeOH (15 mL). The NaOMe was added to the reaction. The reaction immediately turns a light yellow color that becomes darker (brown to black) over time. The reaction was stirred for 24 h at  $60 \text{ }^\circ\text{C}$ , resulting in a black solution. Separately, anhydrous Ni(II)OAc<sub>2</sub> (424 mg, 2.4 mmol, 1.0 equiv) was dissolved in anhydrous MeOH (20 mL). At the 24 h reaction mark, the addition of the Ni(II) solution was started at a rate of  $20 \text{ mL h}^{-1}$ , such that the Ni(II) solution is added over 1 h. The reaction becomes a “sol–gel” during the addition, such that stirring was significantly impeded. The reaction was stirred at  $60 \text{ }^\circ\text{C}$  for an additional 23 h, to give a total reaction time of 48 h. Glacial acetic acid (1 mL in 10 mL MeOH) was added rapidly by syringe to quench any remaining base before addition of the oxidant. The reaction vessel was shaken to homogenize the contents. Iodine (609 mg, 2.4 mmol, 2.0 equiv of oxidant) in MeOH (10 mL) was added in one portion. The

reaction was allowed to stir for several hours at 60 °C, at which point the iodine color had faded from the solution, the “sol–gel” had become a fine suspension, and the reaction suspension settles upon removal of stirring. The solids were collected on a 0.45 µm nylon filter. Without allowing the slurry to filter completely between washes, the product was washed three times each with MeOH, distilled water, methanol again, and finally ether. The resulting lustrous grey-blue material was allowed to dry on the filter before being dried under high vacuum overnight. After crushing in an agate mortar and pestle, the powder was dried again under high vacuum to remove any trapped solvent to give PP. A portion of this material was annealed in a borosilicate vial on a hotplate at 160 °C in air for 1 h to give AP.

**Characterization:** The content of carbon, hydrogen, and sulfur was obtained by Atlantic Microlabs (2400 II analyzer, PerkinElmer for CH, 1108 analyzer, Carlo Erba for S). The analysis of nickel and sodium was carried out on an inductively coupled plasma optical emission spectrometer (OPTIMA 7300 DV, PerkinElmer) by the Renewable Bioproducts Institute at Georgia Tech. Each sample was dissolved in concentrated nitric acid and diluted with deionized water prior to analysis. XPS was performed on the powder samples using a Thermo K-Alpha XPS (Thermo Fisher Scientific Inc.). TGA on PVDF was performed using Pyris 1 Thermogravimetric Analyzer (PerkinElmer) under nitrogen. SEM images were obtained using the SU-8230 tool (Hitachi). The melting point of PVDF was obtained on a Q200 Differential Scanning Calorimeter (TA Instruments) and taken to be at the point of maximum heat flow. TGA coupled with MS was performed by the NETZSCH Applications Laboratory Thermoanalytical Section on a NETZSCH STA 449F1 Jupiter coupled with an NETZSCH QMS 403 Aeolos MS via a transfer line kept at 300 °C. Samples were run in a 25 µL aluminum crucible under a constant flow of Argon (70 mL min<sup>-1</sup>). The heating profile was 40–160 °C at 10 K min<sup>-1</sup>, isothermal at 160 °C for 60 min, and 160–600 °C at 10 K min<sup>-1</sup>. Ion traces were normalized to the noise in the signal during the end of the isothermal hold (34–71 min). SEM images were obtained using the Hitachi SU-8230 tool (Hitachi).

**Film Fabrication and Annealing:** A composite film was obtained by blending the ETT powder with a polymer matrix to form a dispersion. First, PVDF (Sigma Aldrich, Weight average molecular weight (MW) ≈180 000) was dissolved in DMSO (Amresco) at 80 °C for 4 h under continuous stirring in an Erlenmeyer flask to form a 10 mg mL<sup>-1</sup> solution. Next, 40 mg of ETT powder was added to 1 mL of the PVDF/DMSO solution with 10 zirconia beads (diameter = 1 mm) in a microvibration mill for 30 min (MSK-SFM-12M, MTI Corporation). The dispersion was pipetted out and 35 µL was drop-cast on 1 cm × 1 cm pretreated glass substrates (pretreatment of glass substrates involves sequential cleaning with deionized water, acetone, and isopropyl alcohol for 3 min each and placement in oxygen plasma for 5 min). Films were obtained by drying in a vacuum oven at 50 °C for 30 min to give PF. Four gold contact pads (1 mm × 1 mm, ≈100 nm thick) were then deposited on the prepared films using a shadow mask in an e-beam evaporator. All films were 5–10 µm thick as measured with a profilometer (Dektak XT, Bruker). Several samples (films) were prepared to capture sample-to-sample variations in TE properties generating representative error bars that are reported as the standard deviation. For the annealing post-treatment process, films were placed on an aluminum block and heated on a hot plate set to 160 °C in a fumehood. After 1 h, samples were removed from the hot plate and allowed to cool to room temperature over a 30 min period in air to give AF, following which TE measurements were performed.

**TE Measurements:** Micromanipulators with tungsten tips were used to make electrical contact to the gold contact pads and in-plane electrical conductivity was acquired using the four-probe Van der Pauw technique. Samples were placed on a temperature-controlled Peltier stage using thermal grease on the backside of the substrate to ensure good thermal contact. The Seebeck coefficient was measured by suspending the sample between two temperature-controlled Peltier units (separated ≈3 mm) and applying a series of temperature differences up to ΔT = 10 °C between the stages. The TE voltage was measured between two contact pads on separate stages using the probe tips, while the temperature of each pad was measured with a K-type thermocouple in close proximity

to the probe tips. Voltage and temperature data were acquired using a Keithley 2700 DMM with a 7708 Mux card via a LabVIEW interface. The Seebeck coefficient was extracted as the slope of the V versus ΔT plot.

## Supporting Information

Supporting Information is available from the Wiley Online Library or from the author.

## Acknowledgements

R.M.W.W. and A.K.M. contributed equally to this work. This work was supported by Cambridge Display Technology and the Air Force Office of Scientific Research under Award FA9550-15-1-0145. R.W. acknowledges support from the DoD's National Defense Science and Engineering Graduate (NDSEG) Fellowship, 32 CFR 168a. A.K.M. acknowledges support from the Qatar Foundation's Qatar Research Leadership Program (QRLP) Fellowship. The authors acknowledge experimental apparatus support from the Institute for Electronics and Nanotechnology (IEN) and the Center for Organic Photonics and Electronics (COPE) at Georgia Tech.

## Conflict of Interest

The authors declare no conflict of interest.

## Keywords

composite films, ethenetetrathiolates, n-type conductor, organic thermoelectrics, thermal annealing

Received: May 11, 2018

Revised: June 15, 2018

Published online: July 26, 2018

- [1] G. H. Kim, L. Shao, K. Zhang, K. P. Pipe, *Nat. Mater.* **2013**, *12*, 719.
- [2] T. O. Poehler, H. E. Katz, *Energy Environ. Sci.* **2012**, *5*, 8110.
- [3] O. Bubnova, X. Crispin, *Energy Environ. Sci.* **2012**, *5*, 9345.
- [4] O. Bubnova, Z. U. Khan, A. Malti, S. Braun, M. Fahlman, M. Berggren, X. Crispin, *Nat. Mater.* **2011**, *10*, 429.
- [5] S. Wang, H. Sun, U. Ail, M. Vagin, P. O. Å. Persson, J. W. Andreasen, W. Thiel, M. Berggren, X. Crispin, D. Fazzi, S. Fabiano, *Adv. Mater.* **2016**, *28*, 10764.
- [6] R. A. Schlitz, F. G. Brunetti, A. M. Glaudell, P. L. Miller, M. A. Brady, C. J. Takacs, C. J. Hawker, M. L. Chabiny, *Adv. Mater.* **2014**, *26*, 2825.
- [7] B. Russ, M. J. Robb, F. G. Brunetti, P. L. Miller, E. E. Perry, S. N. Patel, V. Ho, W. B. Chang, J. J. Urban, M. L. Chabiny, C. J. Hawker, R. A. Segalman, *Adv. Mater.* **2014**, *26*, 3473.
- [8] C. J. Vineis, A. Shakouri, A. Majumdar, M. G. Kanatzidis, *Adv. Mater.* **2010**, *22*, 3970.
- [9] C. Kittel, P. McEuen, *Introduction to Solid State Physics*, J. Wiley, Hoboken, NJ **2005**.
- [10] B. Russ, A. Glaudell, J. J. Urban, M. L. Chabiny, R. A. Segalman, *Nat. Rev. Mater.* **2016**, *1*, 16050.
- [11] A. M. Glaudell, J. E. Cochran, S. N. Patel, M. L. Chabiny, *Adv. Energy Mater.* **2015**, *5*, 1401072.
- [12] H. Abdalla, G. Zuo, M. Kemerink, *Phys. Rev. B* **2017**, *96*, 241202.
- [13] S. D. Kang, G. J. Snyder, *Nat. Mater.* **2016**, *16*, 252.



- [14] Y. Sun, P. Sheng, C. Di, F. Jiao, W. Xu, D. Qiu, D. Zhu, *Adv. Mater.* **2012**, *24*, 932.
- [15] P. Sheng, Y. Sun, F. Jiao, C. Liu, W. Xu, D. Zhu, *Synth. Met.* **2014**, *188*, 111.
- [16] N. Toshima, K. Oshima, H. Anno, T. Nishinaka, S. Ichikawa, A. Iwata, Y. Shiraishi, *Adv. Mater.* **2015**, *27*, 2246.
- [17] K. Oshima, Y. Shiraishi, N. Toshima, *Chem. Lett.* **2015**, *44*, 1185.
- [18] A. K. Menon, R. M. W. Wolfe, S. R. Marder, J. R. Reynolds, S. K. Yee, *Adv. Mater.* **2018**, *28*, 1801620.
- [19] F. Jiao, C. A. Di, Y. Sun, P. Sheng, W. Xu, D. Zhu, *Philos. Trans. R. Soc., A* **2014**, *372*, 20130008.
- [20] A. K. Menon, E. Uzunlar, R. M. W. Wolfe, J. R. Reynolds, S. R. Marder, S. K. Yee, *J. Appl. Polym. Sci.* **2017**, *134*, 44402.
- [21] Y. Pan, H. K. F. Cheng, L. Li, S. H. Chan, J. Zhao, Y. K. Juay, *J. Polym. Sci., Part B: Polym. Phys.* **2010**, *48*, 2238.
- [22] F. Jiang, L. Zhang, Y. Jiang, Y. Lu, W. Wang, *J. Appl. Polym. Sci.* **2012**, *126*, 845.
- [23] R. Vicente, J. Ribas, P. Cassoux, L. Valade, *Synth. Met.* **1986**, *13*, 265.
- [24] P. N. Nandi, D. A. Deshpande, V. G. Kher, *Thermochim. Acta* **1979**, *32*, 143.
- [25] D. S. Hall, D. J. Lockwood, C. Bock, B. R. MacDougall, *Philos. Trans. R. Soc., A* **2015**, *471*, 201040792.
- [26] E. J. Uzelac, S. C. Rasmussen, *Eur. J. Inorg. Chem.* **2017**, *2017*, 3878.
- [27] E. Tomaszewicz, M. Kotfica, *J. Therm. Anal. Calorim.* **2004**, *77*, 25.
- [28] D. W. Meek, D. K. Straub, R. S. Drago, *J. Am. Chem. Soc.* **1960**, *82*, 6013.